Hindawi
Advances in Civil Engineering
Volume 2022, Article ID 1567182, 16 pages
https://doi.org/10.1155/2022/1567182

Research Article

Experimental and Numerical Analysis of a High-Rise Structure with a Dual FPS Isolation System

Cunkun Duan

School of Civil Engineering, Qingdao University of Technology, Qingdao 266033, China

Correspondence should be addressed to Cunkun Duan; duancunkun@qut.edu.cn

Received 5 December 2021; Revised 23 February 2022; Accepted 24 February 2022; Published 18 March 2022

Academic Editor: André Furtado

Given the issues existing in the isolation technology of high-rise structures, this study displays a thorough examination ponder of three control strategies incorporating numerical and experimental investigation on high-rise structures, which include friction pendulum system (FPS) base isolation, the FPS inter-storey isolation, and the FPS dual isolation. Depending on the third-generation benchmark structure, a scaled 9-storey finite element model is designed, and the matching model of FPS is outlined and fabricated, as required by the geometric similarity criteria. Four typical ground motions and four types of peak ground acceleration (PGA) are considered to investigate the dynamic response of three control strategies. The findings demonstrate that the FPS dual isolation technology can viably smother that acceleration of the top layer of the high-rise structure, and the vibration reduction effect of the substructure will be additionally self-evident. For high-rise structures, the FPS dual isolation technology has a significant vibration decrease impact, not just during minor earthquakes but also even during vast earthquakes. The vibration reduction mechanism of FPS dual isolation technology combines tuned mass damper (TMD) and base isolation technology. Those inertial force drives of the superstructure suppress response from claiming substructure, and same time, substructure is the form of base isolation, which extends that structural period segregates the seismic vitality. The structural deformation can be spread between the lower isolation storey and the upper isolation storey, which effectively limits the floor displacement of the structure. The FPS dual isolation does not mainly reduce that essential mode response of the system and suppresses the response of the high-order mode, which will be the primary reason behind the tremendous vibration decreased impact of the long-period structure. Eventually, it is demonstrated that the finite element model can simulate the dynamic response of the FPS dual isolation system with acceptable accuracy and is suitable for further parametric analysis and comparison by comparing the numerical analysis with the experimental findings.

1. Introduction

Inter-storey isolation technology and base isolation technology have fabulous isolation performance for conventional seismic structure systems [1–4]. The height-width ratio of the base isolation structure is stipulated in China's seismic design code. That is, it should not be greater than 4 [5]. With the increment in height-width ratio, the overall overturning moment of high-rise structure decreases, and the lateral displacement angle increases. Due to the long natural vibration period, it is troublesome to realize an excellent isolation impact using base isolation for high-rise structures. When the high-rise isolated structure experiences a strong dynamic earthquake, the structural deformation is mainly the first-order vibration mode, and the high-order vibration mode is involved, including bending deformation and shear deformation. 111 West 57th Street Tower in New York has reached a super height-width ratio of 24. The super height-width ratio buildings will have problems such as insufficient structural stiffness, out-of-limit displacement index, the tension of vertical members, and zero stress zone of foundation, which makes the structural seismic analysis and designs more and more complex [6].

The inter-storey isolation technology is a new isolation method developed in practice based on base isolation technology. The isolation bearing is installed in the middle storey of the structure to control the seismic response of the system. It can be applied in some unsuitable designs for base

isolation technology, such as offshore platforms where isolation rubber bearings will be corroded by seawater; massive horizontal displacement of isolation storey will impact structural design. Besides, it is easy to install base isolation devices in new buildings, but it is complicated and costly for retrofit applications, excavation, and temporary supports. Installing the isolation system on the roof is relatively inexpensive and straightforward and will not cause damage. Using inter-storey isolation technology, the acceleration response of the structure can be adequately controlled, and the deformation between storeys is mainly concentrated in the isolation storey. The additional storey can be added to the existing system without increasing the base shear. Of course, inter-storey isolation technology also has disadvantages. When using inter-storey isolation, the deformation of the high-rise structure is concentrated on the isolation layer, which will cause irreversible damage to the isolation layer, and the isolation layer cannot recover by itself. When the high-rise isolation structure encounters strong dynamic load, the isolation bearing may be pulled or unstable due to excessive deformation, and the rubber bearing may be damaged due to overturning moment. So far, there are few application examples of inter-storey isolation technology in high-rise structures [7–14].

To further improve the isolation capacity and continuously optimize the isolation performance on the above basis, the dual isolation system appears to be the combination of base isolation and inter-storey isolation methods. The dual isolation system can disperse the seismic force to two isolation storeys, solve the phenomenon of excessive tensile stress in a single isolation storey, make the upper and lower isolation storeys work together, and overcome the contradiction between consuming seismic force and large height-width ratio.

Mega-sub-control method proposed by Wen-Chyr Chai [15] of the University of California in 1996 is the most punctual hypothesis of the dual isolation system. The theoretical principle is that the whole structure is separated into several substructures, and each substructure is composed of connected frames and isolation bearings. It is equivalent to that the substructure becomes a base isolation form, which solves the problems of overturning and torsion of high-rise structure caused by too large aspect ratio and gives the system with large aspect ratio the ability to resist large earthquakes. Therefore, this technology has the advantages of damping, energy dissipation, and foundation isolation.

The friction pendulum system (FPS) has been utilized in engineering since it was initially developed by Professor Zayas of the University of California, Berkeley, in 1985 [16–19]. There is a joint in the sliding block of the FPS, which keeps the sliding block horizontal when it slides along the slideway. The slideway has the same radius of curvature as the slide surface and is coated with low friction materials, such as polytetrafluoroethylene (Teflon). When the earthquake action exceeds the static friction, the FPS makes the superstructure move through the movement of the spherical sliding surface. The horizontal force of the bearing is the resultant force of the friction of the sliding surface and the restoring force of the superstructure rising along the slideway. The period and stiffness of the isolation system can be controlled by choosing the appropriate radius of curvature and the dynamic friction coefficient, which contains the damping property. As shown in Figure 1, the cross section of the FPS is illustrated, in which the direction with the sliding surface facing upward is generally used for base isolation, while the path with the sliding surface facing downward is usually used for inter-storey isolation. The FPS is placed between the structure and the foundation or between the superstructure and the lower frame. It can reduce the lateral force and the horizontal vibration transmitted to the system so that the system will not be damaged under earthquake excitations [20–40].

Given the issues existing in the high-rise structures, this study studies the dual isolation technology based on friction pendulum system (FPS) combined with base isolation technology and inter-storey isolation technology. As a strategy to control the seismic response of high-rise structures with large height-width ratio, the FPS dual isolation technology can overcome the problem that the isolation bearing of the FPS base isolation structure deforms too much during the earthquake, resulting in the tensile damage of the bearing, which makes the system prone to overturning and collapse. Furthermore, it decreases FPS collision damage caused by sizeable sliding displacement in the FPS inter-storey isolation structure and improves the anti-overturning ability of high-rise structures. It solves the limitation of using isolation and damping technology in high-rise structures and has the advantage of self-resetting. The three control strategies' acceleration vibration reduction effect and displacement response are compared by numerical analysis.

2. FEMs of FPS and FPS Dual Isolation Structure

2.1. Mechanical Model of FPS. The mechanical model of FPS is shown in Figure 2. $W = mg$ is the total weight of the isolated building; $m = (m_{iso} + \sum_{i=1}^{N} m_i)$ is the total mass of the inter-storey isolation building; m_{iso} is the mass of the isolation floor; m_i is the mass of the ith floor; and g is the gravity acceleration.

Based on the principle of static equilibrium of bending moment at the center of the arc, the horizontal force can be written as a combination of restoring force and friction force.

$$FR\cos\theta - WD - fR = 0 \Longrightarrow F = \frac{WD}{R\cos\theta} + \frac{f}{\cos\theta}. \quad (1)$$

When θ is small, the unidirectional horizontal force-deformation relation of FPS is given as follows:

$$F = \frac{WD}{R} + \mu W \operatorname{sgn}(\dot{\theta}). \quad (2)$$

$D = R\sin\theta$ is the horizontal slipping displacement, and R is the radius of curvature of FPS; $N = W\cos\theta$ is the normal force of slider; $f = \mu N \operatorname{sgn}(\dot{\theta})$ is the friction force, where μ is the friction coefficient and θ refers to the rotation angle of the slider relative to the vertical symmetry axis of the slide, which is positive in the anticlockwise direction.

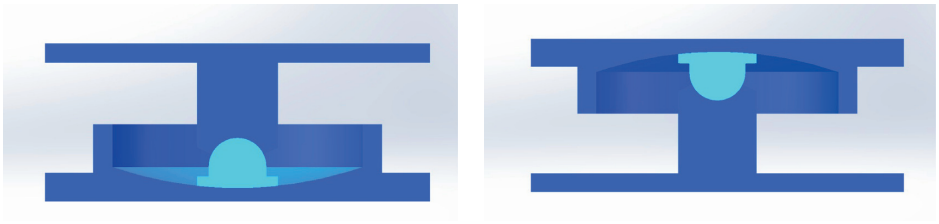

(a) (b)

Figure 1: Friction pendulum system. (a) For base isolation. (b) For inter-storey isolation.

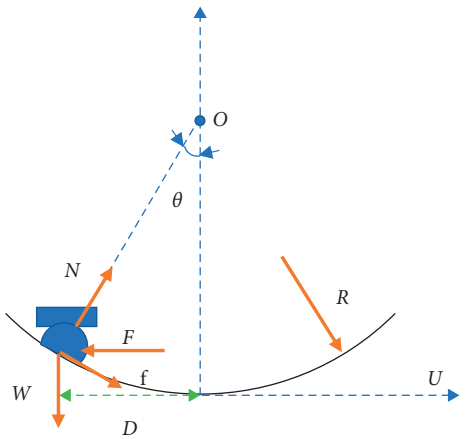

Figure 2: Calculation model of FPS.

According to (2), the hysteretic curve of FPS can be obtained and shown in Figure 3.

$k_h = (W/R)$ is the restoring stiffness of FPS, $k_i = \mu W/d_y$ is the initial stiffness of FPS, and d_y is the yield displacement of FPS, which is the small displacement value of the FPS sliding against static friction. The equivalent stiffness of FPS is as follows:

$$k_{eff} = \frac{F}{D_d} = \frac{W}{R} + \frac{\mu W}{D_d}, \tag{3}$$

where D_d is the limited displacement value of FPS and k_{eff} is equivalent stiffness of FPS.

2.2. FEM Analysis of FPS. The finite element model of FPS is established by ANSYS, as shown in Figure 4. The test model is shown in Figure 5. The slideway radius of the sliding surface of the bearing is 200 mm, and the design displacement value is ±40 mm. The FPS is simulated by a 20-node hexahedral element (SOLID186), suitable for elastoplastic analysis and contact analysis. The constitutive model is the isotropic elastic model, and the elastic modulus of steel is 2×10^5 MPa. Poisson's ratio is 0.3, and the density is 7.85×10^3 kg/m^3. In ANSYS, the friction coefficient is defined as a constant. The tangential friction of the contact surface follows Coulomb's law, and the static friction coefficient is the same as the dynamic friction coefficient, so the correlation between friction coefficient and velocity cannot be considered.

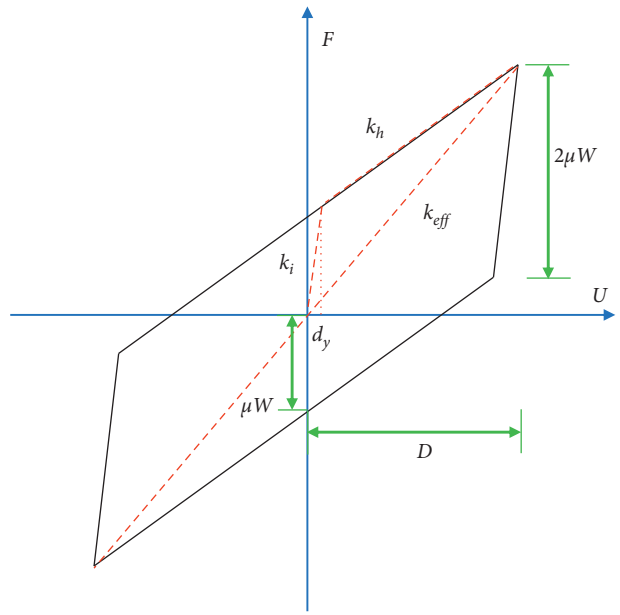

Figure 3: Hysteretic model of FPS.

As shown in Figure 6, the experimental and numerical simulation results of FPS are listed. The finite element model well simulates the mechanical behavior of FPS, and the hysteretic curve is entire and steady, which confirms the rightness of the theoretical mechanical model and the accuracy of the finite element results. The equivalent stiffness of the finite element analysis results is higher than the theoretical calculation value, whereas the equivalent stiffness of the test results is lower.

2.3. FEM of FPS Dual Isolation Structure. The finite element models for the FPS base isolation structure, the FPS inter-storey isolation structure, and the FPS dual isolation structure are established using finite element software ANSYS Workbench to compare and validate the experimental results. As shown in Figure 7, the model column and plate are modeled by the BEAM188 element and SHELL181 element, respectively. The SOLID186 element models the FPS and shake table, which simulates the loading of ground motions by applying a force load to the shake table. Each component of the FPS uses a "Joint" to determine the form of joint movement, and friction contact is defined between the contact surfaces using the CONTA174 element and the

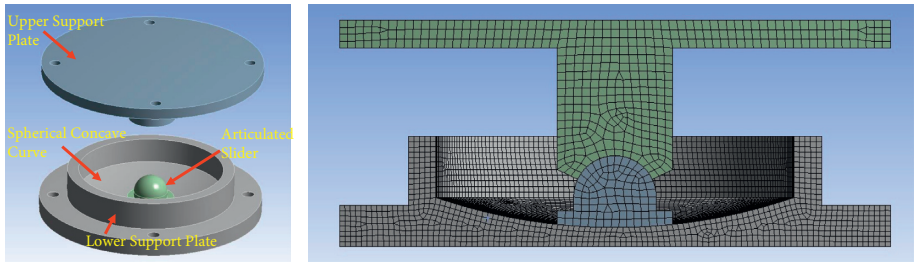

Figure 4: Finite element model of FPS.

Figure 5: FPS.

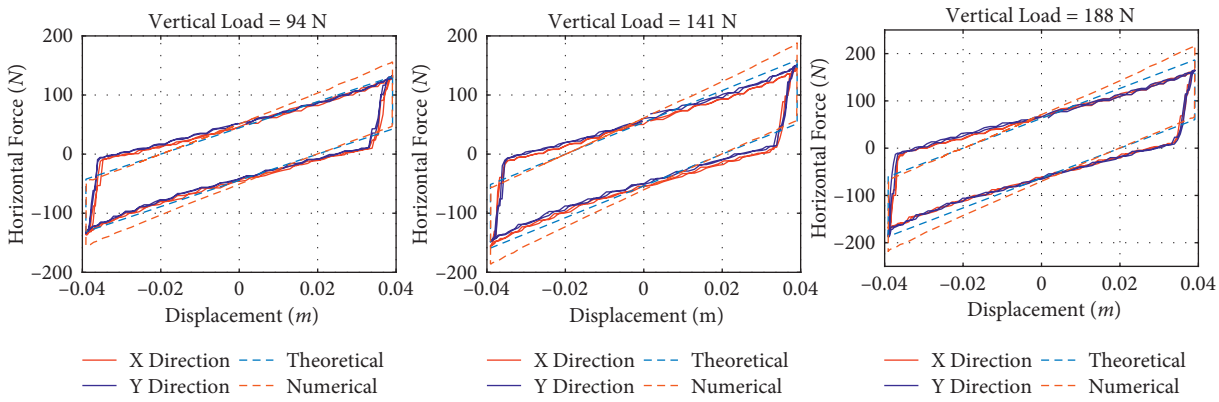

Figure 6: Hysteretic curve of numerical simulation and test results.

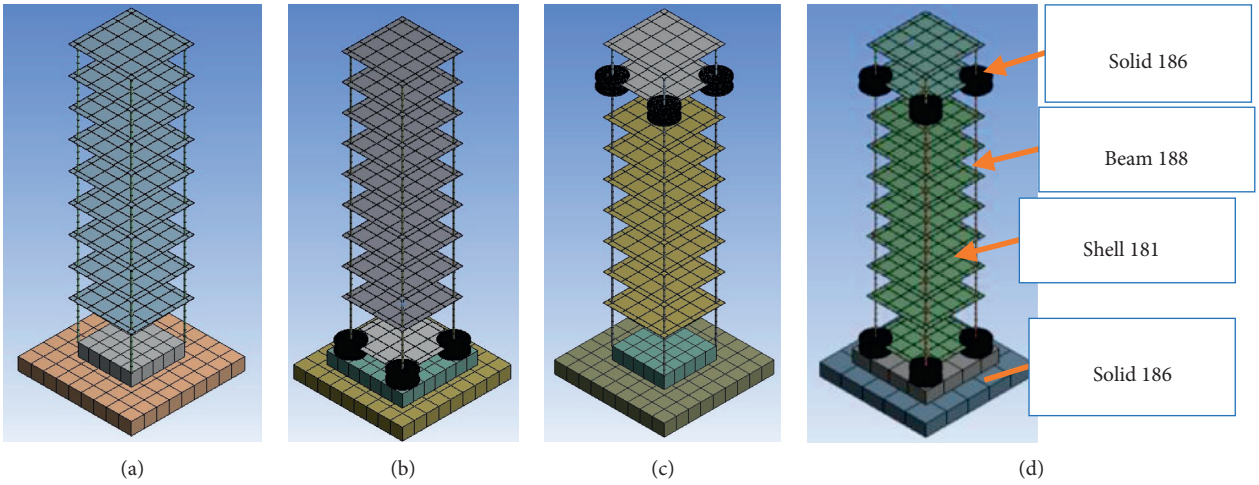

Figure 7: Finite element models of the structure FPS isolation system. (a) Primary structure. (b) FPS base isolation structure. (c) FPS inter-storey isolation structure. (d) FPS dual isolation structure.

TARGE170 element. Asymmetric behavior is adopted, the augmented Lagrangian algorithm is adopted for contact coordination, and the contact stiffness ratio is defined as 0.1. Nodal projection normal from contact is adopted for contact detection between the slider and the lower support plate, and nodal normal to target is adopted for contact detection between the slider and upper support plate. A 345 MPa steel is used as the material of FPS, shake table, column, and plate. The size of the finite element model is determined to be 0.5 m × 0.5 m, and the total height is 2.065 m. The first storey is 0.305 m high, and the other storeys are 0.22 m high, and thus, the height-width ratio is 4.13.

2.4. Ground Motions. Four ground motions with important horizontal components are selected from the Pacific Earthquake Engineering Research Center (PEERC) database, including 1940 El Centro ground motion, 1952 Taft ground motion, 1979 Imperial Valley ground motion, and 1994 Northridge ground motion, as shown in Table 1. At the same time, the peak ground acceleration (PGA) values for the structural response of the structure FPS isolation system under different seismic intensities are 0.1 g, 0.15 g, 0.2 g, and 0.25 g, respectively. Figure 8 depicts earthquake records in the X-direction.

3. Dynamic Property of FPS Dual Isolation Structure

The model's dynamic characteristics are examined first. The primary structure, the FPS base isolation structure, the FPS inter-storey isolation structure, and the FPS dual isolation structure's mode frequencies are all found using the modal analysis. Tables 2 and 3 present a summary of the findings. The natural frequencies of the numerical simulation findings are in perfect accord with those of the test, as can be seen from the data. The primary structure's first natural frequency is 2.25 Hz. The fundamental natural frequency of the structure is reduced after using FPS base isolation, and the first natural frequency is 2.14 Hz; the first natural frequency of the structure is reduced to 1.60 Hz after using FPS inter-storey isolation technology; and the first natural frequency of the structure is further reduced to 1.53 Hz after using FPS dual isolation technology.

The mode participation mass coefficient is only related to vibration modes. Using the orthogonality of different vibration modes, the sum of the mode participation mass coefficient is 1, which indicates that the mode participation mass coefficient is equivalent to a weight distribution coefficient, and the mode participation mass coefficient directly indicates the proportion of the influence of corresponding vibration modes in all vibration modes. The participation mass coefficient of the structure's first vibration mode grows dramatically once the control technique is implemented, whereas the participation mass coefficient of other vibration modes declines. The first vibration mode of the FPS dual isolation structure has a participation mass coefficient of 99.64%, which means that the isolation strategy can fast enhance the weight of the first vibration mode effect while reducing the contributions of the second and higher vibration modes.

Table 1: Selected ground motions.

No.	Excitation	Magnitude
1	1940 Imperial Valley, El Centro Array #9, 180°	6.95
2	1952 Kern County, Taft Lincoln School, 21	7.36
3	1979 Imperial Valley, El Centro Array#5, 140	6.53
4	1994 Northridge, Sylmar Hospital, 090	5.13

4. FEM Analysis Results

The primary goal of this work is to evaluate the performance of the three control systems by analyzing and comparing the dynamic responses of the FPS base isolation structure, the FPS inter-storey isolation structure, and the FPS dual isolation structure. As a result, structural acceleration and floor displacement are the most important indexes for measuring and assessing seismic performance.

4.1. Time Histories of Structural Response at the Top Floor. The top acceleration of the FPS dual isolation structure is much smaller than that of the other two structures, as shown in Figure 9, and the vibration reduction effect is visible. The FPS dual isolation technology can effectively inhibit high-rise structural reaction, weaken high-frequency seismic waves, and consume seismic energy.

Top floor's acceleration vibration reduction rate = (top floor's peak acceleration of the primary structure–top floor's peak acceleration of the FPS isolation structure)/top floor's peak acceleration of the primary structure × 100%. Table 4 shows that the acceleration vibration reduction rate of FPS base isolation technology is concentrated between 7% and 50%, the acceleration vibration reduction rate of FPS inter-storey isolation technology is mainly reflected between 19% and 60%, and the acceleration vibration reduction rate of FPS dual isolation technology is mainly reflected between 38% and 65%. The vibration reduction effect is superior to that of other vibration control technologies. The results reveal that the FPS dual isolation technology is more resilient and effective than the FPS base isolation technology and that it incorporates the benefits of both the FPS base isolation and FPS inter-storey isolation technologies. In addition, the FPS dual isolation technology increases high-rise structure vibration reduction and controls structural deformation on two isolation storeys.

The vibration reduction effects of the first two control methods are lost in the case of a small earthquake, and the acceleration response increases, indicating that the FPS cannot slide completely in the case of a small earthquake, and thus cannot achieve the vibration reduction effect and reduce energy consumption. In the case of small earthquakes, the FPS dual isolation technology reduces vibration by more than 60%, and in the case of large earthquakes, it reduces vibration even more. It demonstrates that the FPS dual isolation technique improves the structure's ability to deal with major and super large earthquakes, as well as having a superior application outlook.

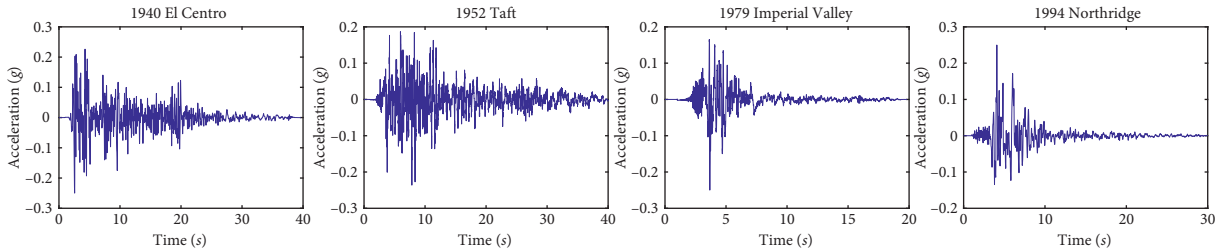

Figure 8: Ground motions.

Table 2: *X*-direction mode of structure/(Hz).

Mode	1	2	3	4	5
Primary structure	2.25 (2.20)	8.17 (8.10)	17.99 (14.70)	28.51 (27.00)	41.05 (42.97)
FPS base isolation structure	2.14 (2.02)	7.74 (4.98)	17.04 (16.34)	30.95 (23.16)	41.52 (39.90)
FPS inter-storey isolation structure	1.60 (1.31)	8.68 (4.95)	20.09 (15.66)	29.57 (22.69)	41.14 (39.14)
FPS dual isolation structure	1.53 (1.24)	8.15 (4.81)	19.09 (15.10)	28.91 (21.34)	40.38 (38.52)

Note. Test value is in brackets.

Table 3: *X*-direction mode participation mass coefficient of structure/(%).

Mode	1	2	3	4	5
Primary structure	89.11	8.92	1.79	0.19	0.00
FPS base isolation structure	96.96	2.63	0.33	0.07	0.00
FPS inter-storey isolation structure	98.64	1.08	0.006	0.28	0.00
FPS dual isolation structure	99.64	0.19	0.12	0.02	0.00

On the one hand, the vibration reduction mechanism of the FPS dual isolation structure is the combination of tuned mass damper (TMD) and base isolation technology. The superstructure is equivalent to a mass block. The inertial force when the superstructure and the lower structure produce relative displacement produces the opposite force on the lower structure through the horizontal force of the upper friction pendulum system to control the acceleration response and deformation of the lower structure. On the other hand, the substructure and base isolation bearings form a base isolation structure, which prolongs the fundamental period of the isolation system and isolates part of the seismic energy. Finally, the amount of seismic energy is consumed by friction on the contact surface of the friction pendulum system. These three factors work together to progress the vibration reduction effect of FPS dual isolation technology.

4.2. The Amplification Factor of Floor Acceleration. The amplification or reduction in the superstructure's input acceleration to the table can be reflected in the floor acceleration amplification factor. The acceleration amplification factor curve is shown in Figure 10. By comparing the two technologies, it is discovered that the FPS dual isolation technology can successfully manage the superstructure's acceleration. In addition to the top floor's outstanding vibration reduction effect, the bottom structure's acceleration is effectively restrained, the floor acceleration change is steady, and the floor acceleration amplification factor varies between 0.5 and 2. The FPS dual isolation technique has a good vibration reduction effect on high-rise building structures, as evidenced by the large reduction in the acceleration response of the top level.

4.3. Acceleration Transfer Function. The acceleration Fourier spectrum is shown in Figure 11. The FPS dual isolation structure's acceleration Fourier spectrum amplitude reduces dramatically, suggesting that the frequency component corresponding to the vibration mode frequency is suppressed during ground motion transmission from the shaking table to the structure. The top acceleration transfer function curve is shown in Figure 12. The acceleration transfer function of the first-order vibration mode of the FPS dual isolation high-rise structure has a substantially smaller amplitude than the other two structures' first-order vibration modes. Using the FPS dual isolation technology, the amplitude of the high-order mode's acceleration transfer function is likewise lowered.

The above analysis reveals that during the transmission process between the FPS base isolation structure and the FPS inter-storey isolation structure, the seismic energy components with similar vibration mode frequencies of the FPS base isolation structure and the FPS inter-storey isolation structure are amplified, while the seismic energy components with similar vibration mode frequencies of the FPS dual isolation structure are not significantly strengthened, and other frequency components are effectively isolated.

High-order vibration modes have a far greater impact on the FPS foundation isolation structure and FPS inter-storey isolation structure than they do on the FPS dual isolation structure. To manage the total seismic response of high-rise structures, FPS dual isolation technology decreases the seismic response of basic vibration modes of high-rise structures and effectively suppresses the seismic response of high-order vibration modes of high-rise structures.

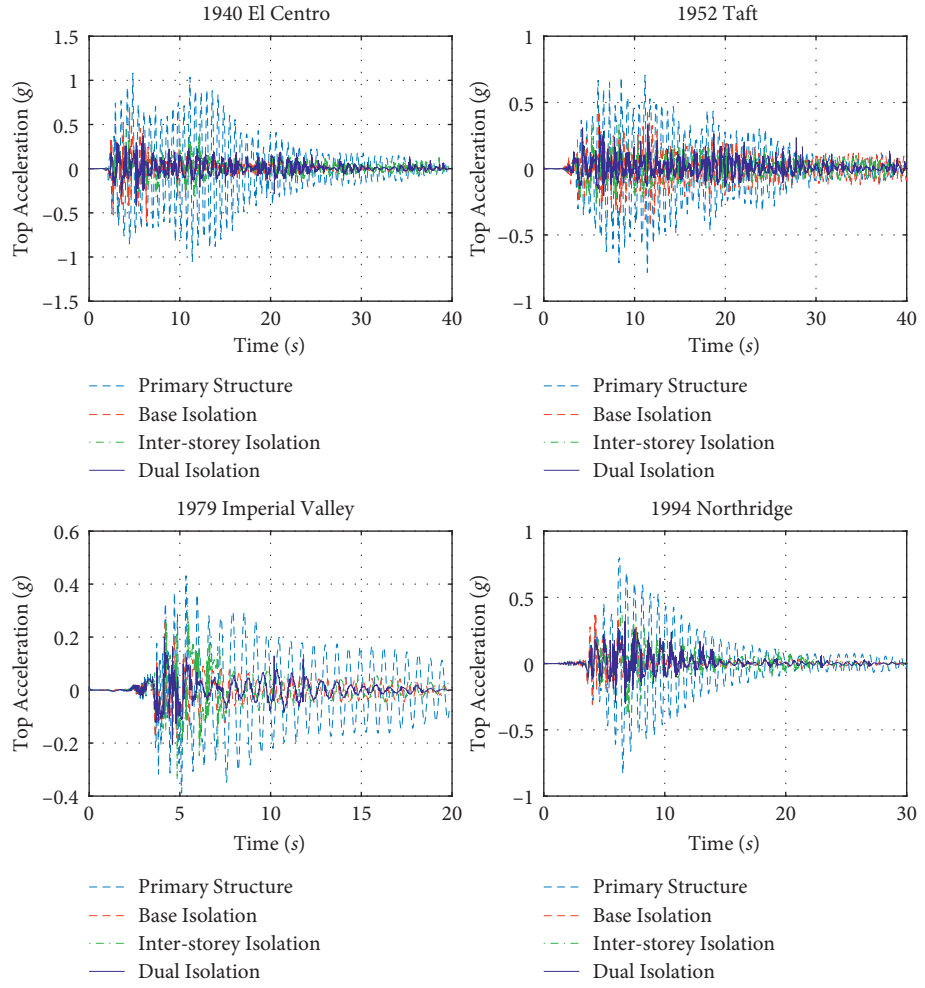

Figure 9: Top acceleration time-history curve.

Table 4: Top acceleration vibration reduction rate of the structure FPS isolation system/(%).

	PGA (g)	1940 El Centro	1952 Taft	1979 Imperial Valley	1994 Northridge
FPS base isolation structure	0.1	28.22	12.00	29.35	29.35
	0.15	41.40	36.39	11.53	23.56
	0.2	21.19	49.38	7.20	17.65
	0.25	35.56	43.39	41.39	27.78
FPS inter-storey isolation structure	0.1	25.81	22.37	28.74	28.74
	0.15	31.64	39.10	41.85	55.41
	0.2	41.27	45.99	29.55	30.99
	0.25	59.14	54.83	19.59	51.86
FPS dual isolation structure	0.1	51.98	42.94	38.16	38.16
	0.15	54.50	56.47	55.20	41.55
	0.2	49.36	64.53	50.53	54.00
	0.25	61.98	57.79	52.59	61.62

4.4. Floor Displacement. The floor displacement curves are depicted in Figure 13. The floor displacement increases as the floor position rises. When Taft, Imperial Valley, and Northridge ground motions are applied, the floor displacement of the FPS base isolation structure is less than that of the FPS inter-storey isolation structure, and structural deformation is localized primarily on the isolation layer. The FPS inter-storey isolation technology has poor control on the floor displacement and even exceeds the floor displacement of the primary structure. The FPS dual isolation structure, in comparison with the other two control systems, can successfully regulate the structure's floor displacement, and the control effect is visible. It demonstrates that the FPS dual isolation technique can effectively avoid floor displacement while maintaining the superstructure's acceleration control effect.

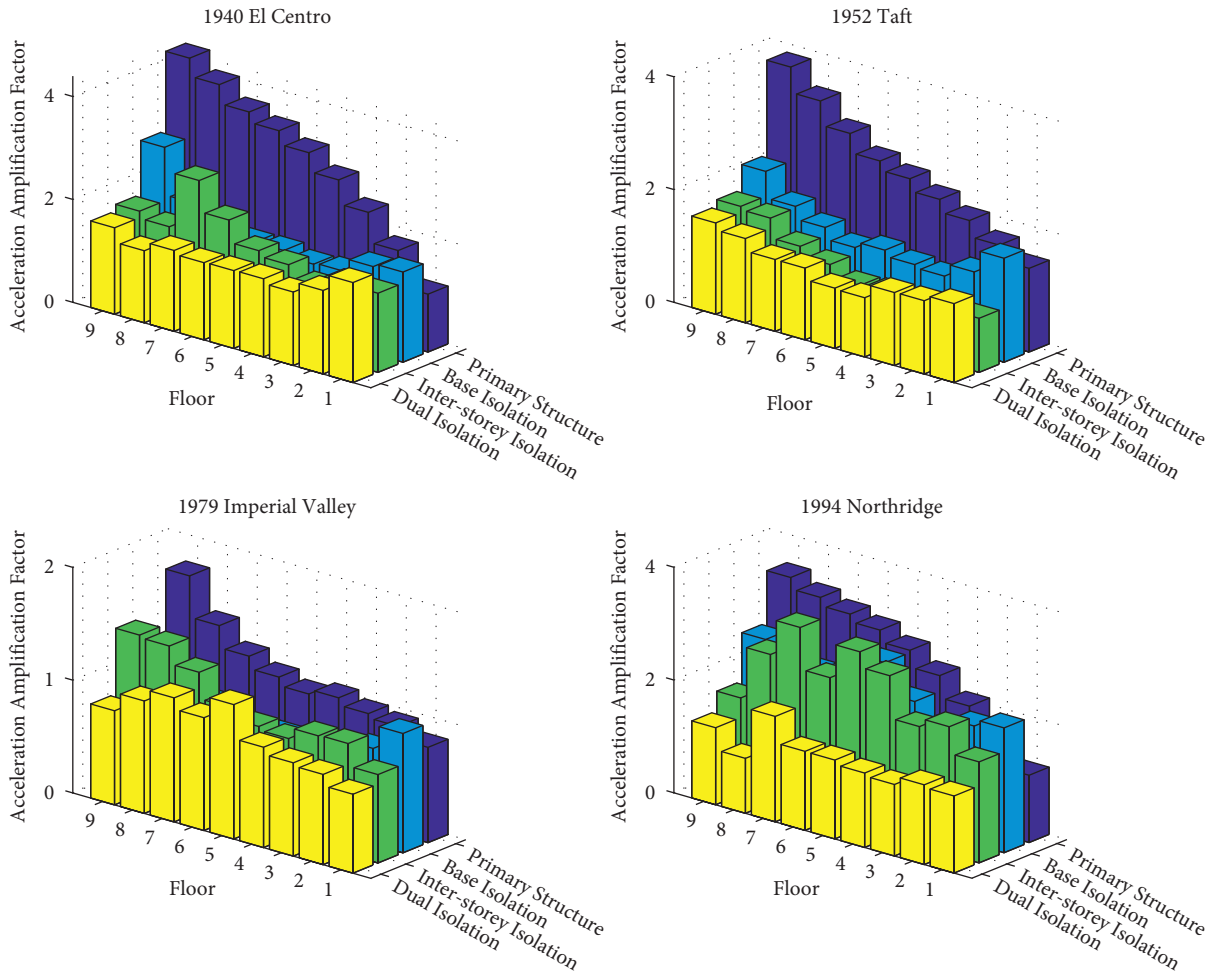

Figure 10: Acceleration amplification factor curve.

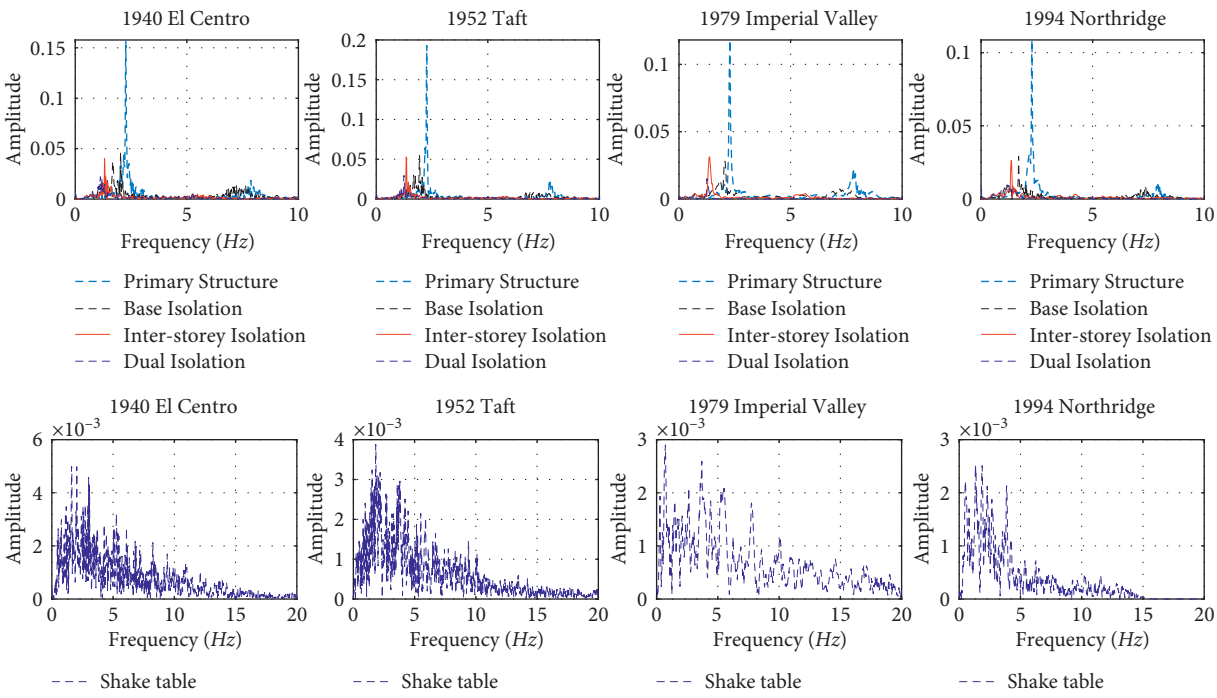

Figure 11: Fourier spectrum of top floor acceleration and shake table acceleration.

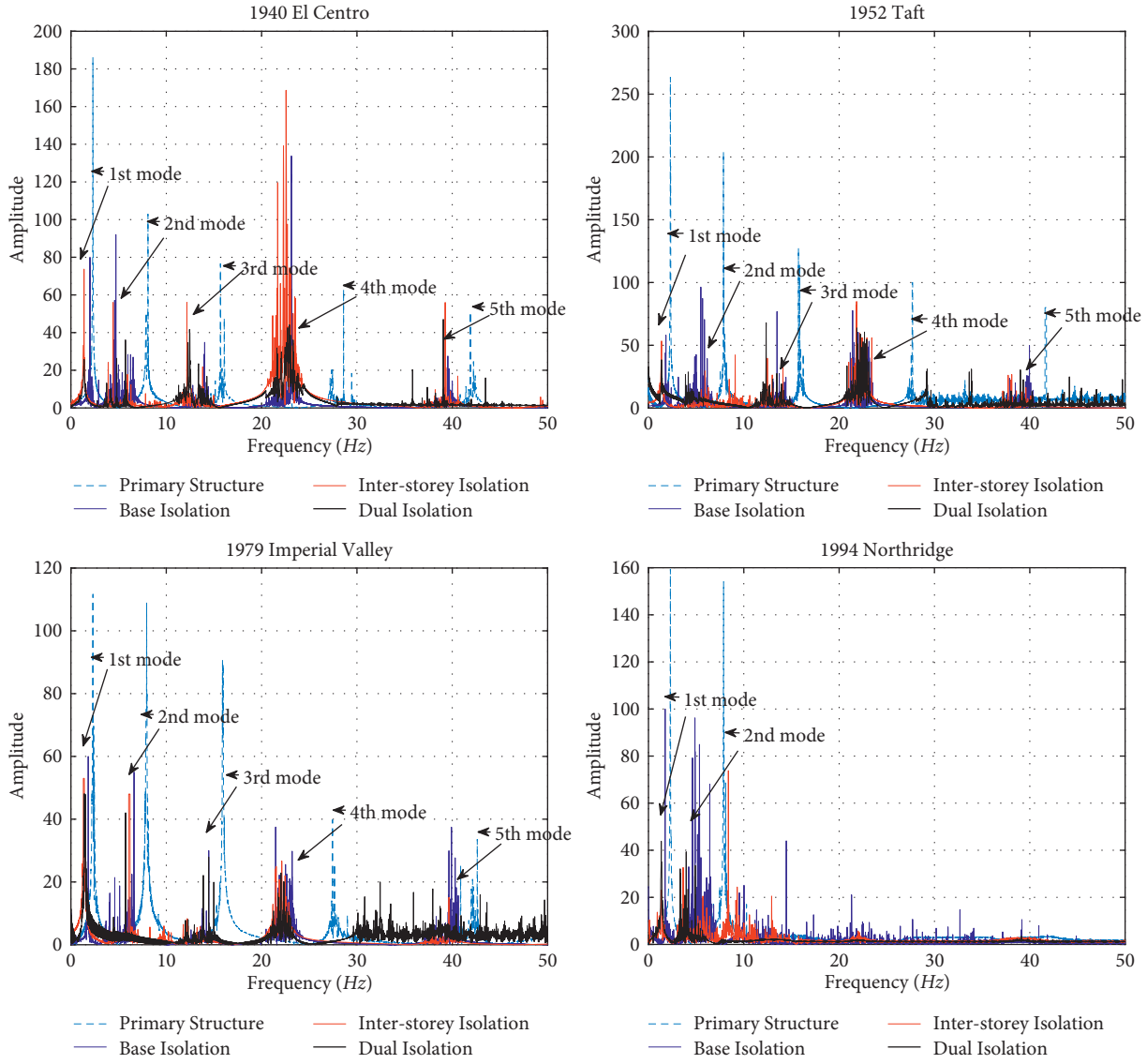

Figure 12: Top acceleration transfer function curve.

4.5. Peak Displacements of the FPS Isolators. As shown in Table 5 and Figure 14, the peak displacements and displacement time-history curves of the FPS are shown. It should be noted that, like the TMD device, the superstructure of the FPS inter-storey isolation structure can be comparable to a considerable mass. The inertia force of the superstructure inhibits the seismic response of the lower structure under the action of seismic load, resulting in an effective structural vibration reduction effect. However, its cost is to sacrifice the deformation of the isolation storey of the superstructure. When the deformation of the isolation storey exceeds the friction pendulum system's design stroke, the superstructure can be inverted and unstable, necessitating precautionary measures.

The peak displacement of the isolation storey of the FPS base isolation structure and the peak displacement of the FPS inter-storey isolation structure, respectively, are significantly greater than the peak displacement of the lower isolation storey and the peak displacement of the upper isolation storey of the FPS dual isolation structure, as shown in the table. The FPS dual isolation technique increases vibration reduction and distributes structural distortion across the lower and higher isolation storeys, thereby minimizing the deformation of the isolation storey. Furthermore, the lower isolation storey's displacement peak is substantially higher than the upper isolation storey's displacement peak, and the structural deformation is mostly caused by the lower isolation storey's deformation. It improves the deficiency of FPS inter-storey isolation technology and avoids the bending deformation of high-rise structures under seismic load, resulting in mostly shear deformation of the structure. Furthermore, the FPS displacement time-history curve demonstrates that after the seismic load has been removed, the upper and lower support plates of the FPS will naturally return to the center of the FPS, demonstrating that the FPS dual isolation technology has superior self-resetting capacity.

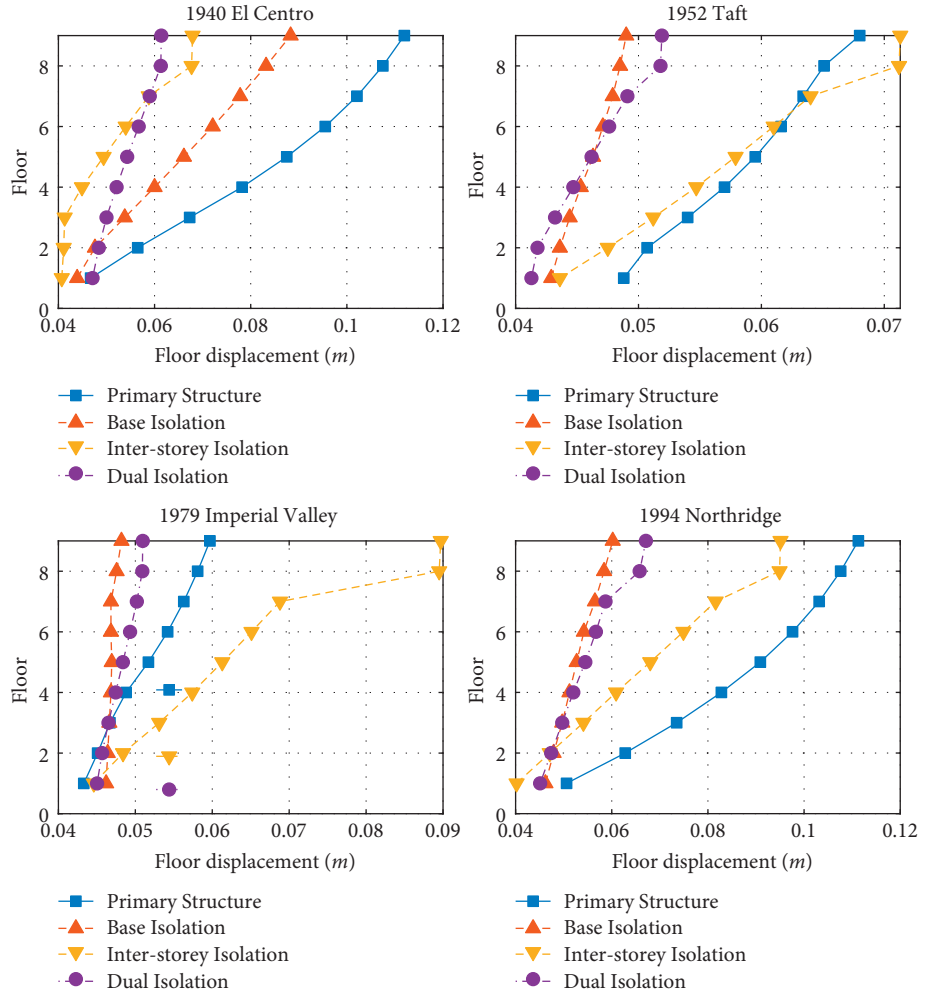

Figure 13: Floor displacement curve.

Table 5: Peak displacements of the FPS isolator/m.

		PGA	1940 El Centro	1952 Taft	1979 Imperial Valley	1994 Northridge
FPS inter-storey isolation structure		0.1 g	0.0132	0.0015	0.007	0.0030
		0.15 g	0.0149	0.0093	0.0011	0.0013
		0.2 g	0.0240	0.0126	0.0032	0.0050
		0.25 g	0.0247	0.0151	0.0192	0.0117
FPS base isolation structure		0.1 g	0.0090	0.0043	0.0016	0.0049
		0.15 g	0.0120	0.0099	0.0037	0.0120
		0.2 g	0.0311	0.0104	0.0041	0.0244
		0.25 g	0.0344	0.0091	0.0071	0.0234
FPS dual isolation structure	Upper isolation storey	0.1 g	0.0035	0.0027	0.0008	0.0027
		0.15 g	0.0080	0.0039	0.0010	0.0029
		0.2 g	0.0105	0.0038	0.0011	0.0035
		0.25 g	0.0143	0.0041	0.0014	0.0048
	Lower isolation storey	0.1 g	0.0102	0.0061	0.0034	0.0101
		0.15 g	0.0133	0.0055	0.0049	0.0157
		0.2 g	0.0142	0.0080	0.0055	0.0155
		0.25 g	0.0171	0.0103	0.0082	0.0162

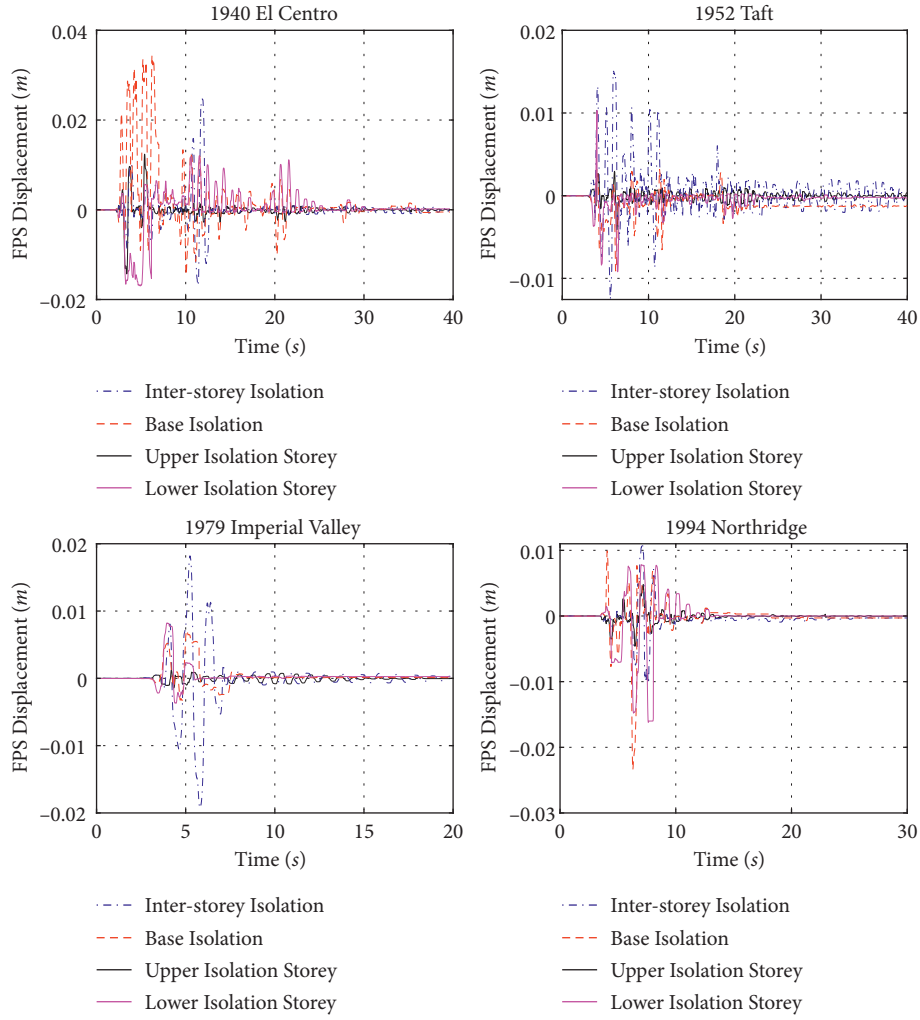

Figure 14: Displacement curve of the FPS isolator.

5. Shaking Table Tests of the Control Scheme

5.1. Test Model Setup. The test structure is a scaled model of the third-generation benchmark structure [40]. The original structure's dimension is 9.15 m × 9.15 m in planar and 37.17 m in height. The structure consists of 9 storeys, 5.49 m in the first storey and 3.96 m in the other storeys. The original structure belongs to the high-rise structure range. The structural floor is a combination of steel and concrete. The beam is made of a 248 MPa steel beam, the column is a 345 MPa steel column, and the section is made of a wide-flange I-shaped section. The first storey of the structure has a mass of 28ton, the mass from the second storey to the eighth storey is 27ton each, the mass of the ninth storey is 29ton, and the total structural weight is 246ton.

The shake table III of Quanser Inc., 71.1 cm × 71.1 cm two-way input shaker, is used in the test. The maximum seismic excitation is 1.0 g at a load of 100 kg, and the X- and Y-direction travel is 10.8 *cm,* respectively. Considering factors such as shake table performance, operating conditions, and lifting capacity, the geometric similarity constant S_l of the model structure is chosen to be 1/18; secondly, considering the vibration level, the load capacity of the table, and the model materials, the stress similarity constant is chosen to be $S_\sigma = 0.2$. Therefore, the acceleration similarity constant is $S_a = 1.5$, the mass similarity constant is $S_m = 4 \times 10^{-4}$, and the similarity ratios of the model used in the test are summarized in Table 6.

According to the model similarity constant, the mass of the first storey is 11.2 kg, the mass from the second storey to the eighth storey is 10.8 kg, the mass of the ninth storey is 11.6 kg, and the total weight is 98.4 kg. The size of the test model is determined to be 0.5 m × 0.5 m, and the total height is 2.065 m. The first storey is 0.305 m high, and the other storeys are 0.22 m high, and thus, the height-width ratio is 4.13. The photograph and design sketch of the structural test model is shown in Figure 15.

Before this study, the shaking table test of the FPS inter-storey isolation structure was accomplished. When the friction pendulum system is mounted on the top level, the test results show that significant vibration reduction may be accomplished. The investigation will not be carried out in great detail in this study. Figure 16 depicts the FPS base isolation structure, FPS inter-storey isolation structure, and

Table 6: Scale factors of the model.

	Quantity	Scale transformation	Scale factor	Remarks
Physical characteristics	Length	S_l	1/18	Control size
	Area	$S_s = S_l^2$	1/324	
	Linear displacement	$S_X = S_l$	1/18	
	Strain	S_ε	1.0	
Material properties	Stress	$S_\sigma = S_E$	0.20	
	Elastic modulus	S_E	0.20	Control material
	Density	S_ρ	2.4	
Load	Force	$S_F = S_E S_l^2$	6.17×10^{-4}	
	Line load	$S_P = S_E S_l$	0.011	
	Mass	$S_m = S_\rho S_l^3$	4×10^{-4}	
	Stiffness	$S_k = S_E S_l$	0.011	
Dynamic characteristics	Time	$S_t = (S_l/S_a)^{1/2}$	0.20	
	Frequency	$S_f = (S_a/S_l)^{1/2}$	5.20	
	Acceleration	S_a	1.5	Control test

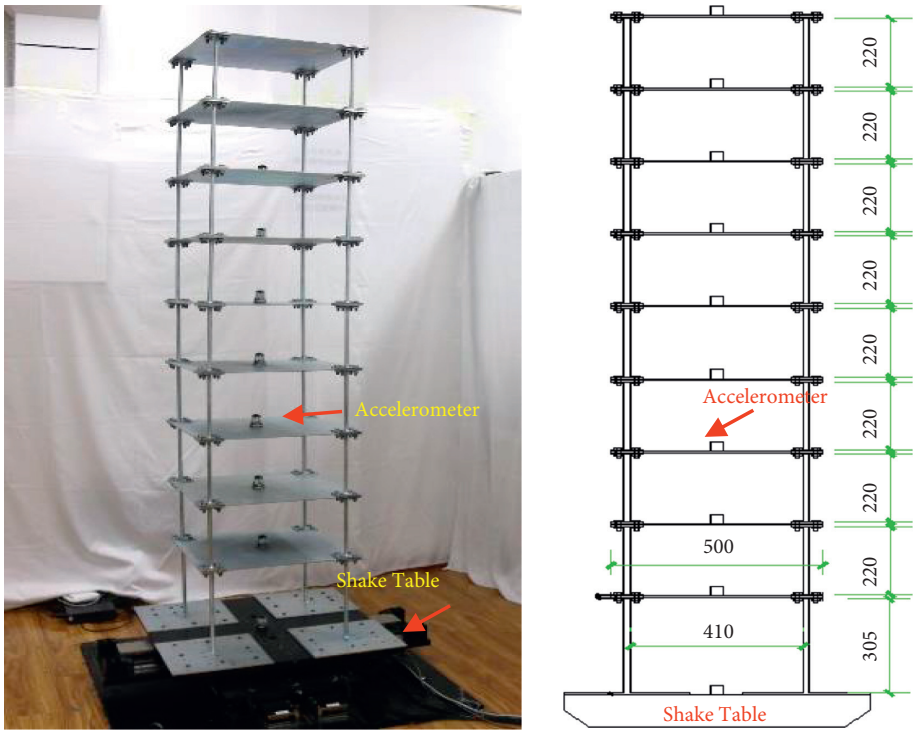

Figure 15: Photograph of tested model structure on the shake table.

FPS dual isolation structure schematically. The vibration reduction impact is obvious as the foremost self-evident when the FPS inter-level isolation storey is placed on the 8th floor, according to the previous experiment. The isolation level for further analysis and comparison to the base isolation approach is appropriately chosen as the 8th floor. Besides, 10 Lord Inc. Wireless sensors are set within the center of each floor and on the shake table to record the absolute acceleration response.

5.2. Results and Analysis. The numerical analysis and experimental findings of the top floor's acceleration time history, the RMS values of the primary structure's floor

(a) (b) (c)

Figure 16: Test model. (a) FPS base isolation structure. (b) FPS inter-storey isolation structure. (c) FPS dual isolation structure.

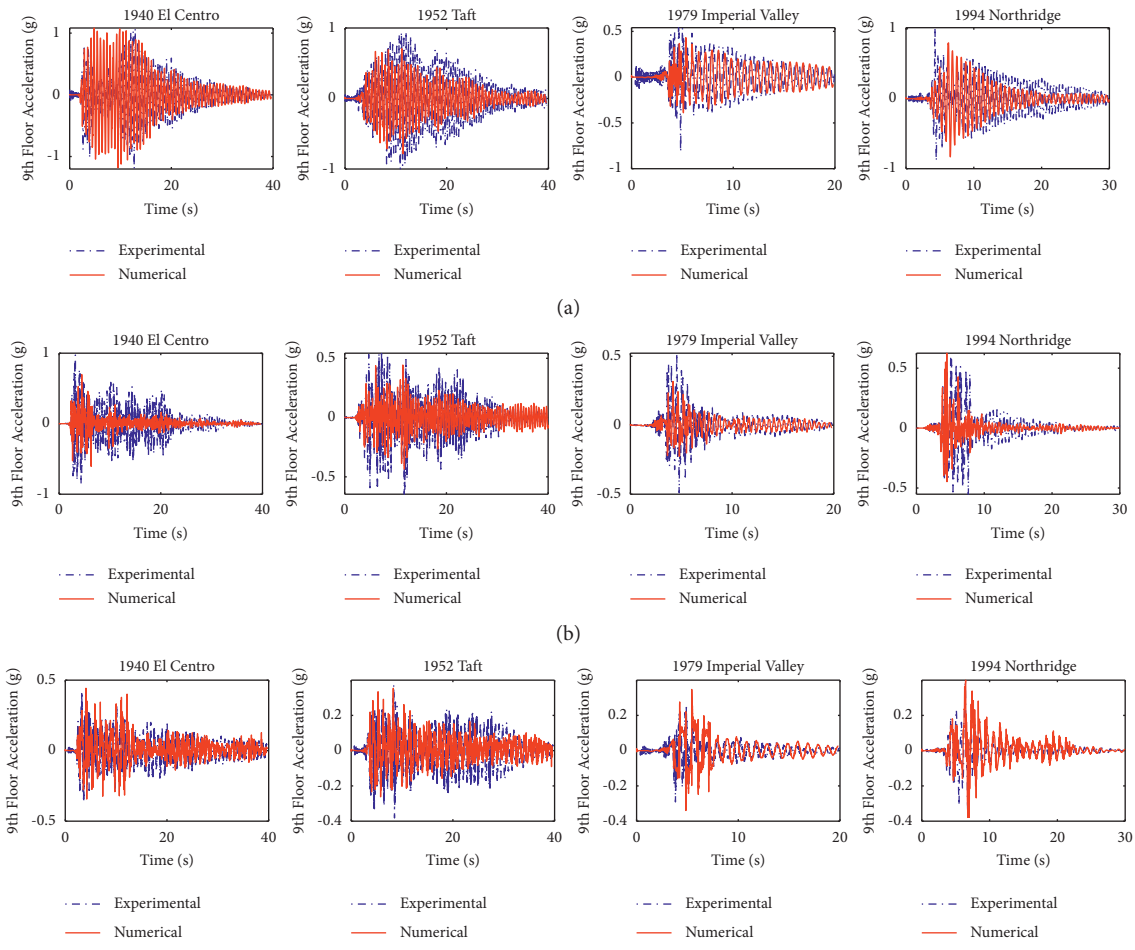

(a)

(b)

(c)

Figure 17: Continued.

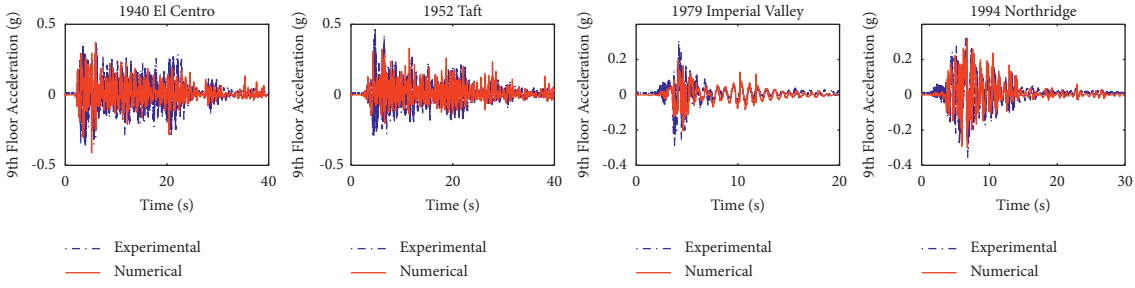

(d)

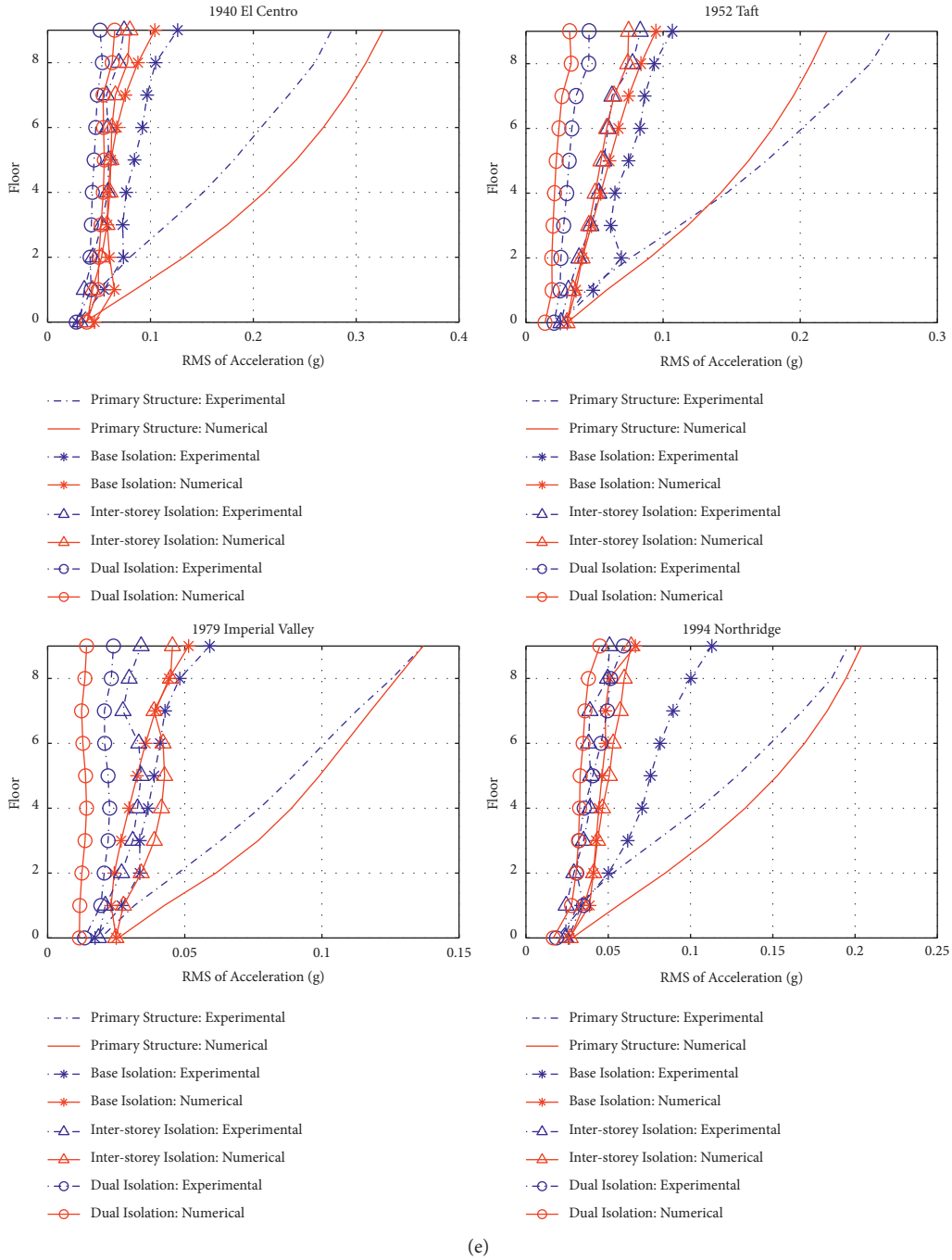

(e)

FIGURE 17: Comparison of experimental and numerical results in (a) primary structure; (b) FPS base isolation structure; (c) FPS inter-storey isolation structure; (d) FPS dual isolation structure; and (e) RMS values of floor acceleration.

acceleration, the FPS base isolation structure, the FPS inter-storey isolation structure, and the FPS dual isolation structure are displayed in Figure 17. The finite element model is proven to accurately reproduce the seismic response of the structure FPS isolation system and primary structure. In most situations, the numerical and experimental results remarkably agree with the same trend.

6. Conclusion

In this study, another FPS isolation control technology, specifically FPS dual isolation technology, is compared for FPS base isolation technology and FPS inter-storey isolation technology. The finite element model of the FPS dual isolation structure is established. The absolute acceleration and displacement response of each floor of the model structure is obtained through numerical analysis. Compared with the FPS base isolation structure and the FPS inter-storey isolation structure, the top acceleration vibration reduction rate, floor acceleration amplification factor, floor displacement, acceleration transfer function, and peak displacements of the FPS are analyzed. Secondly, the effectiveness of the finite element model is verified by comparing the test results. The main conclusions are as follows:

(1) The vibration reduction effect of FPS dual isolation technology is concentrated between 38% and 65%. The vibration reduction impact of high-rise structures is great when compared to other control methods, and the structure's capacity to manage major and super large earthquakes is increased.

(2) There are two parts to the FPS dual isolation technology's vibration reduction process. On the one hand, modifying the structural form isolates a portion of the seismic energy. The friction of the contact surface of the friction pendulum system, on the other hand, consumes seismic energy.

(3) The FPS dual isolation technology decreases the seismic response of high-rise structures' basic vibration modes while successfully suffocating the seismic response of high-order vibration modes. As a result, the overall seismic response of high-rise structures is regulated, which is a useful isolation measure.

(4) The FPS dual isolation technology can adequately control the floor displacement of the structure, appropriately distribute the structural deformation to the lower isolation storey and upper isolation storey, effectively limit the isolation storey deformation, reduce the risk of overturning instability and failure of superstructure due to excessive deformation of upper isolation storey, and can be reset by itself.

Data Availability

The data used to support the findings of this study are included within the article.

Conflicts of Interest

The author declares no conflicts of interest.

References

[1] R. S. Jangid and J. M. Kelly, "Base isolation for near-fault motions," *Earthquake Engineering & Structural Dynamics*, vol. 30, no. 5, pp. 691–707, 2001.

[2] M. C. Kunde and R. S. Jangid, "Seismic behavior of isolated bridges: a-state-of-the-art re-view," *Electronic Journal of Structural Engineering*, vol. 3, pp. 140–170, 2003.

[3] V. Zayas, "Earthquake protective column support," *US patent*, vol. 24, 1987.

[4] Y. M. Wu and B. Samali, "Shake table testing of a base isolated model," *Engineering Structures*, vol. 24, no. 9, pp. 1203–1215, 2002.

[5] *GB 50011-2010 Code for Seismic Design of Buildings*, China Architecture & Building Press, Beijing, China, [in Chinese], 2010.

[6] S. H. Eem, H. J. Jung, and J. H. Koo, "Seismic performance evaluation of an MR elastomer-based smart base isolation system using real-time hybrid simulation," *Smart Materials and Structures*, vol. 22, p. 055003, 2013.

[7] Y. Li, J. Li, W. Li, and H. Du, "A state-of-the-art review on magnetorheological elastomer devices," *Smart Materials and Structures*, vol. 23, no. 12, Article ID 123001, 2014.

[8] K. L. Ryan and C. L. Earl, "Analysis and design of inter-story isolation systems with nonlinear devices," *Journal of Earthquake Engineering*, vol. 14, no. 7, pp. 1044–1062, 2010.

[9] Q. Zhou, M. P. Singh, and X. Y. Huang, "Model reduction and optimal parameters of mid-story isolation systems," *Engineering Structures*, vol. 124, pp. 36–48, 2016.

[10] F. Zhou, Y. Zhang, and P. Tan, "Theoretical study on storey isolation system," *China Civil Engineering Journal*, vol. 42, no. 8, pp. 1–8, 2009, [in Chinese].

[11] Y. Zhang, P. Tan, and F. Zhou, "Study on seismic reduction performance and parameter design of newly segmented isolation system," *China Civil Engineering Journal*, vol. 43, no. S1, pp. 270–275, 2010, [in Chinese].

[12] Y. Liu, J. Wu, and M. Donà, "Effectiveness of fluid-viscous dampers for improved seismic performance of inter-storey isolated buildings," *Engineering Structures*, vol. 169, pp. 276–292, 2018.

[13] V. Bolvardi, S. Pei, J. W. van de Lindt, and J. D. Dolan, "Direct displacement design of tall cross laminated timber platform buildings with inter-story isolation," *Engineering Structures*, vol. 167, pp. 740–749, 2018.

[14] W. C. Chai, *Mega-sub Control of High-Rise Buildings*, University of California, Irvine, 1996.

[15] V. Zayas, S. Low, and S. Mahin, "The FPS Earthquake Resisting System: Experimental Report," Report no. UCB/EERC-87/01, Earthquake Engineering Research Center, University of California, Berkeley, 1987.

[16] V. A. Zayas, S. S. Low, and S. A. Mahin, "A simple pendulum technique for achieving seismic isolation," *Earthquake Spectra*, vol. 6, no. 2, pp. 317–333, 1990.

[17] E. Meral, "Determination of seismic isolation effects on irregular RC buildings using friction pendulums," *Structures*, vol. 34, pp. 3436–3452, 2021.

[18] H. Keikha and G. G. Amiri, "Developing a simplified method for analysis and design of isolated structures with the novel quintuple friction pendulum system under bidirectional near-field excitations," *Journal of Vibration and Control*, Article ID 10775463211048261, 2021.

[19] L.-Y. Lu, T.-Y. Lee, and S.-W. Yeh, "Theory and experimental study for sliding isolators with variable curvature," *Earthquake Engineering & Structural Dynamics*, vol. 40, no. 14, pp. 1609–1627, 2011.

[20] C. S. Tsai, W. S. Chen, T. C. Chiang, and B. J. Chen, "Component and shaking table tests for full-scale multiple friction pendulum system," *Earthquake Engineering & Structural Dynamics*, vol. 35, no. 11, pp. 1653–1675, 2006.

[21] P. C. Roussis and M. C. Constantinou, "Experimental and analytical studies of structures seismically isolated with an uplift-restraining friction pendulum system," *Earthquake Engineering & Structural Dynamics*, vol. 35, no. 5, pp. 595–611, 2006.

[22] C. P. Providakis, "Effect of supplemental damping on LRB and FPS seismic isolators under near-fault ground motions," *Soil Dynamics and Earthquake Engineering*, vol. 29, no. 1, pp. 80–90, 2009.

[23] Y. Zhou and P. Chen, "Shaking table tests and numerical studies on the effect of viscous dampers on an isolated RC building by friction pendulum bearings," *Soil Dynamics and Earthquake Engineering*, vol. 100, pp. 330–344, 2017.

[24] L. Landi, G. Grazi, and P. P. Diotallevi, "Comparison of different models for friction pendulum isolators in structures subjected to horizontal and vertical ground motions," *Soil Dynamics and Earthquake Engineering*, vol. 81, pp. 75–83, 2016.

[25] W.-Z. Zheng, H. Wang, J. Li, and H.-J. Shen, "Parametric study of SMA-based friction pendulum system for response control of bridges under near-fault ground motions," *Journal of Earthquake Engineering*, vol. 25, no. 8, pp. 1494–1512, 2021.

[26] M. B. Brito, M. Akiyama, T. Seto, R. Honda, and N. Ishigaki, "Shaking table test of a friction sliding system on a concrete member with variable curvature fabricated by a three-dimensional printer," *Journal of Earthquake Engineering*, pp. 1–27, 2021.

[27] A. Krishnamoorthy, "Finite element method of analysis for liquid storage tank isolated with friction pendulum system," *Journal of Earthquake Engineering*, vol. 25, no. 1, pp. 82–92, 2021.

[28] V. R. Panchal and R. S. Jangid, "Variable friction pendulum system for near-fault ground motions," *Structural Control and Health Monitoring*, vol. 15, no. 4, pp. 568–584, 2008.

[29] B. Wei, Y. Fu, S. Li, and L. Jiang, "Influence on the seismic isolation performance of friction pendulum system when XY shear keys are sheared asynchronously," *Structures*, vol. 33, pp. 1908–1922, 2021.

[30] J. N. Yang, J. Bobrow, F. Jabbari, J. Leavitt, C. P. Cheng, and P. Y. Lin, "Full-scale experimental verification of resetable semi-active stiffness dampers," *Earthquake Engineering & Structural Dynamics*, vol. 36, no. 9, pp. 1255–1273, 2007.

[31] S.-P. Chang, N. Makris, A. S. Whittaker, and A. C. T. Thompson, "Experimental and analytical studies on the performance of hybrid isolation systems," *Earthquake Engineering & Structural Dynamics*, vol. 31, no. 2, pp. 421–443, 2002.

[32] I. Politopoulos, "A review of adverse effects of damping in seismic isolation," *Earthquake Engineering & Structural Dynamics*, vol. 37, no. 3, pp. 447–465, 2008.

[33] L. Di Sarno, A. S. Elnashai, and G. Manfredi, "Assessment of RC columns subjected to horizontal and vertical ground motions recorded during the 2009 L'Aquila (Italy) earthquake," *Engineering Structures*, vol. 33, no. 5, pp. 1514–1535, 2011.

[34] S. Berton, S. Infanti, M. G. Castellano, and H. Hikosaka, "Self-centring capacity of seismic isolation systems," *Structural Control and Health Monitoring*, vol. 14, no. 6, pp. 895–914, 2006.

[35] M. Dicleli and S. Buddaram, "Effect of isolator and ground motion characteristics on the performance of seismic-isolated bridges," *Earthquake Engineering & Structural Dynamics*, vol. 35, no. 2, pp. 223–250, 2006.

[36] C. P. Katsaras, T. B. Panagiotakos, and B. Kolias, "Restoring capability of bilinear hysteretic seismic isolation systems," *Earthquake Engineering & Structural Dynamics*, vol. 37, no. 4, pp. 557–575, 2008.

[37] Z. Xu, X. Du, C. Xu, and R. Han, "Numerical analyses of seismic performance of underground and aboveground structures with friction pendulum bearings," *Soil Dynamics and Earthquake Engineering*, vol. 130, Article ID 105967, 2020.

[38] K. L. Ryan, S. Soroushian, E. M. Maragakis, E. Sato, T. Sasaki, and T. Okazaki, "Seismic simulation of an integrated ceiling-partition wall-piping system at E-defense. I: three-dimensional structural response and base isolation," *Journal of Structural Engineering*, vol. 142, no. 2, Article ID 04015130, 2016.

[39] N. D. Dao, K. L. Ryan, E. Sato, and T. Sasaki, "Predicting the displacement of triple pendulum bearings in a full-scale shaking experiment using a three-dimensional element," *Earthquake Engineering & Structural Dynamics*, vol. 42, no. 11, pp. 1677–1695, 2013.

[40] B. F. Spencer, S. J. Dyke, and H. S. Deoskar, "Benchmark problems in structural control: part I—active mass driver system," *Earthquake Engineering & Structural Dynamics*, vol. 27, no. 11, pp. 1127–1139, 1997.